PNAS RESEARCH ARTICLE | MEDICAL SCIENCES

MiR-155-targeted IcosL controls tumor rejection

Esmerina Tili[a,b,1,2], Hajime Otsu[b,1], Teresa L. Commisso[b], Alexey Palamarchuk[b], Veronica Balatti[b], Jean-Jacques Michaille[b], Gerard James Nuovo[c], and Carlo M. Croce[b,2]

Affiliations are included on p. 9.

Contributed by Carlo M. Croce; received May 3, 2024; accepted June 8, 2024; reviewed by Webster K. Cavenee and Riccardo Dalla-Favera

Elevated levels of *miR-155* in solid and liquid malignancies correlate with aggressiveness of the disease. In this manuscript, we show that *miR-155* targets transcripts encoding IcosL, the ligand for Inducible T-cell costimulator (Icos), thus impairing the ability of T cells to recognize and eliminate malignant cells. We specifically found that overexpression of *miR-155* in B cells of Eμ-*miR-155* mice causes loss of IcosL expression as they progress toward malignancy. Similarly, in mice where *miR-155* expression is controlled by a Cre-Tet-OFF system, *miR-155* induction led to malignant infiltrates lacking *IcosL* expression. Conversely, turning *miR-155* OFF led to tumor regression and emergence of infiltrates composed of IcosL-positive B cells and Icos-positive T cells forming immunological synapses. Therefore, we next engineered malignant cells to express IcosL, in order to determine whether *IcosL* expression would increase tumor infiltration by cytotoxic T cells and reduce tumor progression. Indeed, overexpressing an *IcosL*-encoding cDNA in MC38 murine colon cancer cells before injection into syngeneic C57BL6 mice reduced tumor size and increased intratumor CD8+ T cell infiltration, that formed synapses with IcosL-expressing MC38 cells. Our results underscore the fact that by targeting *IcosL* transcripts, *miR-155* impairs the infiltration of tumors by cytotoxic T cells, as well as the importance of IcosL on enhancing the immune response against malignant cells. These findings should lead to the development of more effective anticancer treatments based on maintaining, increasing, or restoring IcosL expression by malignant cells, along with impairing *miR-155* activity.

immune therapy | immune rejection | microRNA targeting | lymphoma | solid tumor

Significance

We show here that one crucial aspect of microRNA *miR-155* oncogenic activity is the targeting of *ICOSL*, that is needed for the recognition and elimination of malignant cells by CD8-positive T cells. Our data indicate that ICOS–ICOSL immune checkpoint is critical for enhancing the effectiveness of immune therapies, not only for B cell lymphomas, but also for breast, colon, pancreatic, and lung solid tumors. This is supported by our findings that these solid tumors likewise exhibit elevated levels of *miR-155*, suggesting that they may evade the antitumor immune response through similar molecular mechanisms. Coercing cancer cells to express ICOSL, along with reducing *miR-155* levels, could potentially enhance their elimination by immune cells leading to tumor eradication and cure.

Elevated levels of microRNA *miR-155-5p* (*miR-155*) in patients with chronic lymphocytic leukemia (CLL) and other B cell malignancies are associated with the most aggressive forms of the disease and a poor prognosis (1–3). Transgenic mice constitutively overexpressing *miR-155* in B cells (Eμ-*miR-155*) develop lymphoblastic leukemia and high-grade lymphomas (4). Controlled overexpression of *miR-155* in mouse lymphoid tissues similarly causes the development of disseminated B cell lymphomas, confirming that sustained expression of *miR-155* is causative for the development of this type of malignancies (5). Lymphomas regress once *miR-155* has been switched back OFF as previously shown by Babar et al. (5). We were quite surprised, however, by the speed of the tumor regression in these mice once the *miR-155* was turned OFF, and we consequently hypothesized that *miR-155*, in addition to impairing the activity of tumor suppressor genes, such as *Ship1* (5–8) and *Socs1* (9), may also target genes critical for the efficacy of the antitumor immune response. Supporting this hypothesis, the histopathological examination of the regressed tumors revealed an abundant infiltration of T cells, suggesting that *miR-155* may target factors involved in immune recognition and rejection of tumors (this manuscript).

In 2006–2007 we found that *miR-155* is highly expressed not only in B cell malignancies, but also in colon, breast, pancreatic, and lung cancers (10, 11). High levels of *miR-155* expression in these solid malignancies, as in B-cell malignancies, are associated with increased aggressiveness, suggesting that *miR-155* may hinder the recognition of malignant cells by the immune system (12–16). Given that microRNAs can target multiple transcripts simultaneously, the key question regarding the oncogenic effects of *miR-155* in these malignancies is to identify specific target transcripts that encode factors critical for the recognition and elimination of malignant cells by T cells. To address this important question, we focused on immune checkpoints factors expressed by B cells that could potentially be targeted by *miR-155*. Our attention was particularly drawn to Inducible T-cell costimulator Ligand (ICOSL), as bioinformatic analysis revealed a conserved *miR-155* site in the 3′-UTR of *ICOSL* gene that is particularly expressed in B cells. ICOSL acts as the ligand for ICOS/CD278, a T cell–specific surface costimulatory molecule structurally related to CD28 and CTLA-4 (17). *ICOS* expression is induced upon T cell activation (18–20) and is necessary

Author contributions: E.T., J.-J.M., and C.M.C. designed research; E.T., H.O., T.L.C., A.P., V.B., J.-J.M., G.J.N., and C.M.C. performed research; E.T. contributed new reagents/analytic tools; E.T., H.O., T.L.C., J.-J.M., G.J.N., and C.M.C. analyzed data; and E.T., J.-J.M., and C.M.C. wrote the paper.

Reviewers: W.K.C., Ludwig Institute for Cancer Research, Ltd.; and R.D.-F., Columbia University.

The authors declare no competing interest.

[1]E.T. and H.O. contributed equally to this work.

[2]To whom correspondence may be addressed. Email: esmerina.tili@osumc.edu or carlo.croce@osumc.edu.

This article contains supporting information online at https://www.pnas.org/lookup/suppl/doi:10.1073/pnas.2408649121/-/DCSupplemental.

Published July 9, 2024.

for mounting effective T cell-dependent immune responses (21). ICOS-expressing T cells in the germinal centers (GC) are implicated in T-B cell communication and T-cell–dependent B cell responses through ICOS–ICOSL interactions (22–24). ICOSL binding to ICOS induces the formation of immune synapses, T cell activation, and T cell effector functions (25).

In this manuscript, we show that *ICOSL* is a direct target of *miR-155* and that high levels of *miR-155* result in reduction or loss of IcosL expression in two different mouse models of B cell lymphoma. Turning *miR-155* expression OFF after being active, induced a strong lymphocytic infiltration with the formation of immunological synapses between T-B cells through Icos–IcosL interactions. To demonstrate that ICOSL is indeed the critical target of *miR-155* responsible for the elimination of cancer cells and tumor rejection by the immune system, we first overexpressed the coding sequence of *IcosL*, without its 3′-UTR, in a murine MC38 colon cancer cell line derived from C57BL6 mice (26). Our aim was to test the ability of IcosL to induce an immune response targeting tumors induced in mice by the subcutaneous injection of MC38 tumor cells. These cells that are highly mutated, aggressive, and lead rapidly to terminal illness when subcutaneously injected into syngeneic mice. Mice injected with IcosL-overexpressing MC38 cells showed tumors smaller than those found in mice injected with MC38 cells that did not express IcosL. In addition, the tumors derived from IcosL-expressing MC38 cells showed extensive CD8 cell infiltration that aggregated in the areas where IcosL-expressing cells were present as demonstrated by coexpression analyses. Furthermore, we found that CD8-positive cells and IcosL-expressing cells were forming immunological synapses within the tumors.

These results present opportunities for the development of future T-cell-based immune therapies, not only for B cell malignancies but also for other very common tumors that express high levels of *miR-155*, such as breast, lung, pancreatic, or colon cancers. These therapies could focus on enhancing the activity of the ICOS–ICOSL immune checkpoint by either blocking *miR-155* activity or by re-expressing the *ICOSL* gene.

Results

***MiR-155* Activity in Malignant B Cells Impairs T Cell Antitumor Activity at Least in Part by Targeting *ICOSL* Transcripts.** To identify *miR-155* targets involved in antitumor immune response, we first analyzed the effects of *miR-155* on B cell malignancy and T cell infiltration by turning the expression of *miR-155* ON or OFF in lymphocytes of the Nestin-Cre x *miR-155*^{LSLrTA} offspring (5). We first confirmed that the expression of *miR-155* in these mice is induced or repressed by withdrawal or addition of doxycycline in their food, respectively, using in situ hybridization (ISH) (Fig. 1*A*). Turning ON the expression of *miR-155* for 3 mo led to extensive malignant B cell infiltrates in different organs such as the spleen, kidneys, and muscles (Fig. 1 *B*, *Top* panels and *SI Appendix*, Fig. S1), as previously reported (5). When *miR-155* was subsequently turned back OFF for 1 wk, infiltrates remained visible in different organs (Fig. 1 *B*, *Bottom* panels); however, this time the infiltrates were predominantly composed of CD4-positive T cells (brown signal on the *Bottom Right*) and only a few B cells could still be found (Fig. 1 *B*, *Bottom* panel). As B cell tumors regressed, we observed focal infiltrations of T cells expressing Icos (Fig. 1*C*). It is worth noting that the presence of T cells expressing Icos in contrast was rare when *miR-155* was ON (Fig. 1 *C*, *Bottom Left*). These results suggested that high levels of *miR-155* inhibit T cell ingression and that when this microRNA was turned OFF, B cells are eliminated by infiltrating T cells. We thus reasoned that, beside intrinsic mechanisms inducing the apoptosis of malignant B cells, in particular, the derepression of Ship1, that we previously established as a direct target of *miR-155* (6) there should be additional, extrinsic mechanisms also involved in the elimination of malignant B cells, likely through their recognition and elimination by T cells. Among *miR-155* putative targets able to interfere with T cell activity, we then focused on ICOSL because: 1) Our bioinformatic analysis showed a conserved *miR-155* site in the 3′-UTR of *ICOSL* transcripts; 2) ICOSL in B cells serves as the ligand for ICOS/CD278, a T cell–specific surface costimulatory molecule structurally related to CD28 and CTLA-4 (17); 3) ICOS expression is induced upon T cell activation (18–20) and is necessary for mounting effective T cell-dependent immune responses (21); and 4) T cells in the tumor infiltrates were actually expressing Icos once *miR-155* had been turned OFF (Fig. 1*C*). We therefore checked whether *miR-155* could directly target *ICOSL* transcripts. We found that: i) In Raw264.7 macrophages, *miR-155* significantly reduced the activity of a Luciferase reporter construct containing the WT 3′-UTR of human *ICOSL* (Fig. 1*D*). This effect was abolished by mutating the consensus *miR-155* binding site present in *ICOSL* 3′-UTR (Fig. 1*D*); ii) Treating Raw264.7 cells with lipopolysaccharide (LPS), that we have previously shown to increase *miR-155* expression (27), or transfecting these cells with *miR-155*, both reduced the expression of IcosL (Fig. 1*E*); iii) Transfecting *miR-155* into BJAB and NAMALWA Burkitt's lymphoma (BL) cell lines, that do not express *miR-155* (28, 29), reduced the expression of ICOSL (Fig. 1*F*); iv) We and others have previously shown that *miR-155* is highly expressed by CLL cells but not by BL cells (1, 2, 29). A comparative analysis showed an inverse correlation between *miR-155* and ICOSL levels of expression, with BL cells expressing high levels of ICOSL and virtually no *miR-155* versus CLL cells showing high levels of *miR-155* and less ICOSL (Fig. 1*G*); and finally v) transfecting MEC2-CLL cells with a *miR-155*-inhibitor increased the levels of ICOSL on the cell surface as measured by flow cytometry (*SI Appendix*, Fig. S2). Altogether, the above results indicated that *miR-155* activity in malignant B cells may potentially impair T cell infiltration, activation, and antitumor response at least in part through the targeting of *ICOSL* transcripts.

***MiR-155* Activity Leads to Accumulation of Malignant B Cells Lacking *IcosL* Expression.** Given the above results, we next investigated the impact of *miR-155* activity on IcosL expression and tumor progression/regression by turning the expression of *miR-155* ON or OFF in Cre-*Nestin* x *miR-155*^{LSLrTA} mice (5). With *miR-155* ON, the percentage of B cells positive for IcosL in the lymph nodes of Cre-*Nestin* x *miR-155*^{LSLrTA} mice was reduced compared with lymph nodes of wild-type (WT) littermates, based on both flow cytometry (Fig. 2*A*) and IHC analyses. Specifically, in contrast to B splenocytes from WT mice that stained positive for IcosL (Fig. 2*B*, first row), B cell infiltrates in *miR-155*^{LSLrTA} mice with *miR-155* ON for 3 mo completely lacked IcosL expression, and they exhibited a malignant phenotype characterized by their round shape and typical variable intensity of labeling with the B cell marker CD20 (Fig. 2*B*, second row). Although certain cells within these infiltrates stained positive (green) for IcosL, they were not B cells, as morphologically they resembled either endothelial cells or macrophages. Indeed, this was confirmed by costaining for IcosL and CD31 endothelial marker (Fig. 2*B*, third row) or CD163, a macrophage marker (*SI Appendix*, Fig. S3). Turning *miR-155* back OFF for 1 wk after it had been ON for 3 mo led to the disappearance of malignant B cells in Nestin-Cre x *miR-155*^{LSLrTA} mice (Fig. 2*B*, fourth row), also shown in Fig. 1*B* and consistent with previous reports in this mouse model (5). At this timepoint, we found a few CD20-positive cells that presented with the morphology of benign B cells. These B cells expressed IcosL based on the colocalization of CD20 and IcosL signals (Fig. 2*B*, fourth row). As expected, *Socs1*, an established

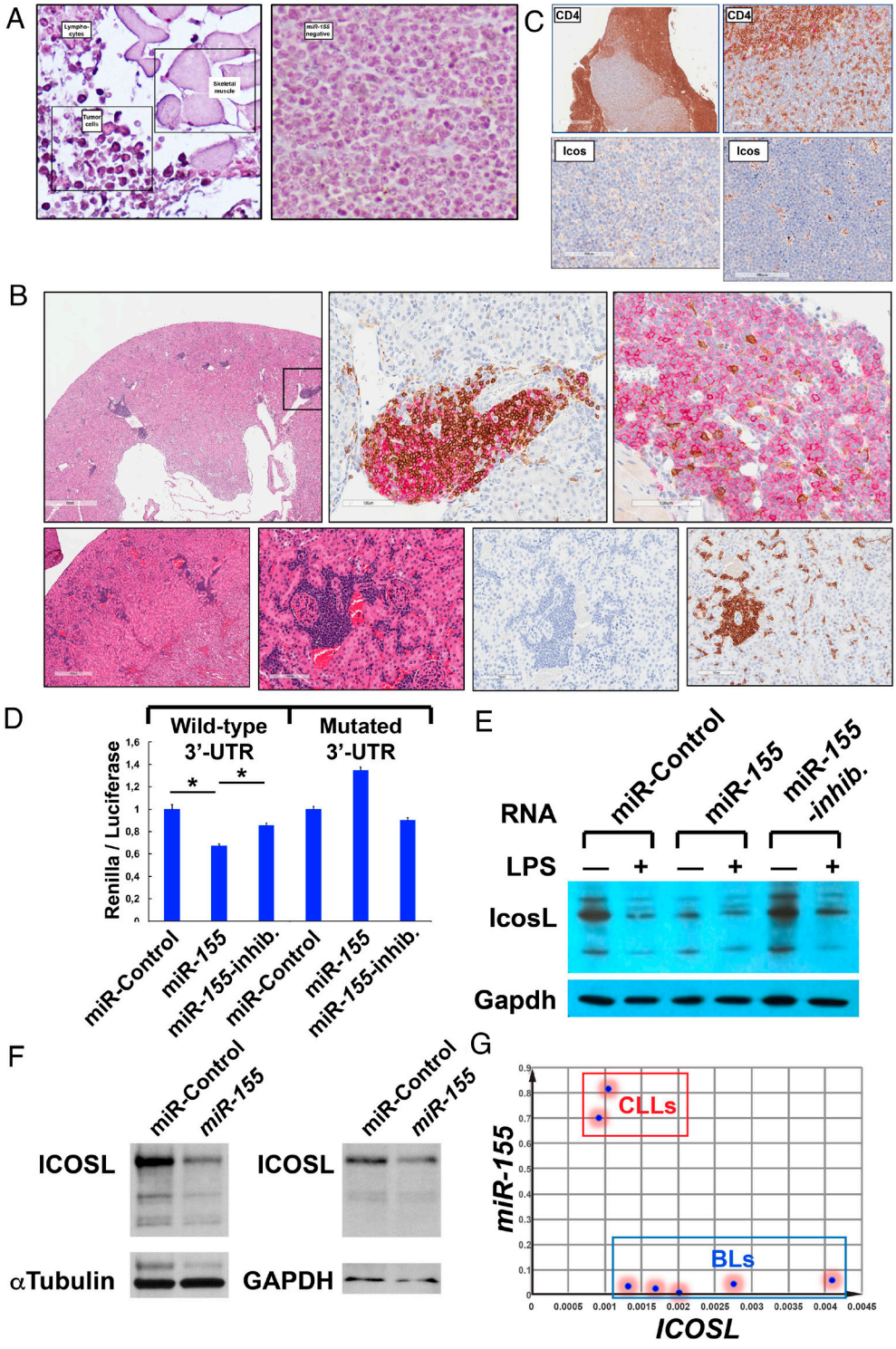

Fig. 1. *MiR-155* impairs T cell antitumor response at least in part by targeting *ICOSL* transcripts. (*A*) Detection of *miR-155* (dark blue) in mice with *miR-155* ON and OFF using ISH. *Left*, *miR-155* detection (dark blue) when this microRNA is turned ON in Nestin-Cre x *miR-155*^{LSLtTA}offspring; *Right*, Lack of *miR-155* expression when this microRNA has been turned OFF in the same mice. (*B*) Tumor infiltrates in mice with *miR-155* ON for 3 mo (*Top* panels) then back OFF for 1 wk (*Bottom* panels). *Top* panels: *Left*: H&E staining of the kidney showing infiltrates (dark blue color); *Middle*: B220 (red signal) and CD4 (brown signal) staining of the infiltrate from the kidney indicated by the square); *Right*: B220 (red signal) and CD4 (brown signal) staining of a skeletal muscle. *Bottom* panels, tumor infiltrates in kidneys. From left to right: H&E staining at low (first panel) and high magnification (second panel); B220 staining (red, third panel, notice lack of B220-positive cells); CD4 staining (brown, fourth panel). (*C*) *Top* panels: *Left*: IHC for CD4 (brown) showing T cell infiltration surrounding a lymph node. *Right*: Magnification of a part of the image on the *Left*. *Bottom* panels: IHC for Icos (brown) on lymphomas with *miR-155* ON (*Left*) and then turned back OFF (*Right*). (*D*) Dual-Luciferase reporter assays performed in Raw264.7 macrophages cotransfected with a Renilla luciferase reporter vector containing the human *ICOSL*-3′-UTR with either the WT *miR-155* binding site or its mutated version, along with either a *miR-Control* RNA, a human *miR-155* RNA, or a human *miR-155*-Inhibitor RNA, as indicated. $n = 6$ replicates/each experimental setting; $P = 5.09182E-07$. (*E*) Raw264.7 cells transfected with either a *miR-Control* RNA, a mouse *miR-155* RNA, or a mouse *miR-155*-Inhibitor RNA, as indicated, were treated with either LPS (100 ng/mL) or the vehicle 24 h after transfection. Two days posttransfection, cell lysates were analyzed by western blot for IcosL expression. GAPDH was used as a loading control. (*F*) Two days after transfection with either a *miR-Control* RNA or human-*miR-155* RNA, BL cell lines BJAB and NAMALWA were analyzed for ICOSL expression by western blotting. α-tubulin and GAPDH were used as loading control. (*G*) Inverse correlation between *miR-155* and *ICOSL* transcripts as measured by qRT-PCR in CLL (MEC1 and MEC2) and BL (NAMALWA, BJAB, RAJI, PH3R1, DAUDI) cell lines.

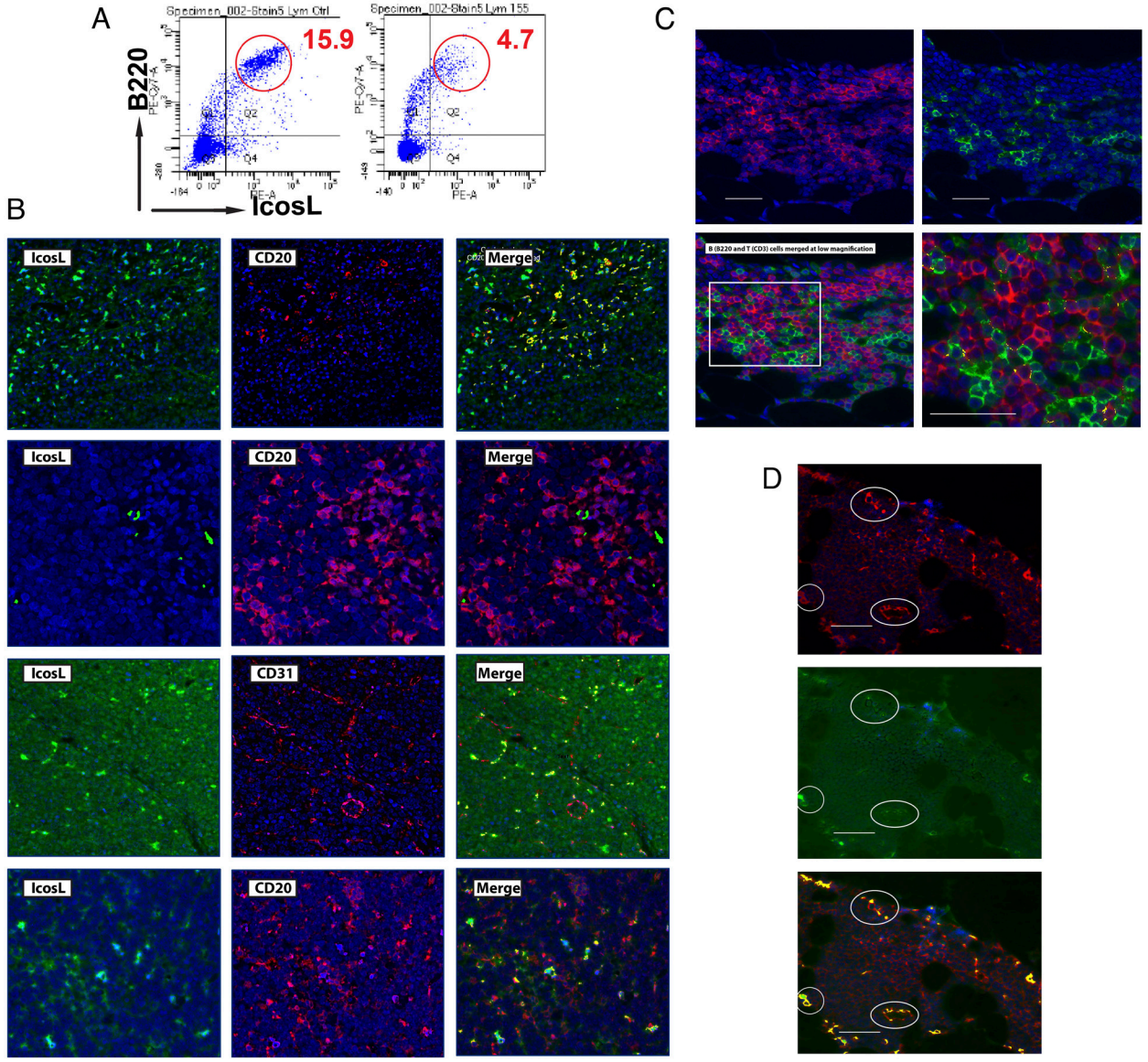

Fig. 2. Turning ON the expression of *miR-155* in lymphocytes of Nestin-Cre x *miR-155*^{LSLtTA} mice leads to development of B cell lymphomas lacking *IcosL* expression, while turning *miR-155* back OFF allows the formation of B (IcosL) - T (Icos) cells synapses mostly located around blood vessels. (*A*) Flow cytometry analyses for B220 and IcosL expression in lymph nodes of littermates with *miR-155* OFF (*Left*) or ON (*Right*) for 2 mo. Representative images. (*B*) First row: IcosL (green; *Left*) and CD20 (red; *Middle*) staining in a WT spleen. Colocalization (yellow; *Right*). Second row: Lack of IcosL (green; *Left*) expression by CD20-positive cells (red; *Middle*) in lymphomas with *miR-155* ON (no yellow signal, *Right*). IcosL-positive cells in the left are distinct from malignant B cells. Third row: IcosL-positive cells (green; *Left*) in lymphomas with *miR-155* ON are CD31-positive (red, *Middle*) with colocalization (yellow; *Right*). Fourth row: A few benign B cells present in the mice with *miR-155* ON then OFF for 1 wk had started to re-express IcosL. CD20 (green; *Left*); IcosL (red; *Middle*); colocalization (yellow; *Right*). Panels are representative of staining of 3 mice/group. (*C*) IHC for B220 (red; *Top Left*), CD3 (green; *Top Right*) in infiltrates from mice with *miR-155* ON for 10 wk then back OFF for 4 d. Scattered B220-CD3 synapses are seen as yellow fluorescence in the pictures at the *Bottom Left* after merging B220-CD3 signals; *Bottom Right* is a magnification of the square in the left picture. (*D*) IHC for Icos (red; *Top*) and IcosL (green; *Middle*) and coexpression (yellow; *Bottom*) in infiltrates from mice with *miR-155* ON for 2 to 3 mo then OFF for 4 d. The immunological synapses between B cells (IcosL) and T cells (Icos) are located mostly around blood vessels (ovals). (Scale bar, 100 μm.)

target of *miR-155* (9), was also reduced and then re-expressed along IcosL in B cell infiltrates with *miR-155* turned ON and then back OFF again, respectively (*SI Appendix*, Fig. S4).

Loss of *IcosL* Expression in Malignant B Cells Impairs the Formation of B-T Cell Immune Synapses and Tumor Immune Surveillance. As shown in Fig. 1*C*, once *miR-155* was turned back OFF and *IcosL* was derepressed, the number of Icos-positive T cells increased along with tumor regression. These T cells showed a focal perivascular accumulation pattern with areas containing a high number of Icos-positive cells (Fig. 1*C*). Thus, the average number of Icos-positive T cells counted automatically in tumors from mice with *miR-155* ON shown in Fig. 1*C* was 5.3/200× microscopic field but increased dramatically to 131/200× microscopic field after *miR-155* was turned back OFF again for 1 wk. Similar results were also obtained in the spleen; however, the difference did not reach statistical significance most probably due to the existence of variable patterns as compared to diffuse pattern of T cell infiltrates (*SI Appendix*, Fig. S5). Nevertheless, the induction of IcosL once *miR-155* was turned back OFF strongly suggested that, in addition to undergoing apoptosis due to the derepression of *Socs1* (*SI Appendix*, Fig. S4) or *Ship1* (5), malignant B cells were also being eliminated through extrinsic mechanisms, likely through their recognition and elimination by T cells. This elimination of malignant B cells was likely facilitated by Icos–IcosL engagement. Namely, when *miR-155* was induced for 10 to 12 wk and then turned OFF for a period as short as 4 d, we found Icos-positive T cells forming immune synapses with IcosL-positive B cells in remaining infiltrates (Fig. 2*C*).

Interestingly, the T (Icos) - B (IcosL) interactions were primarily observed in the vicinity of blood vessels (Fig. 2*D*). The localization of synapses next to blood vessels likely explains the presence of focal areas containing Icos-positive T cells seen in Fig. 1*C* and may also reflect the ability of IcosL-expressing B cells to recruit and activate T cells at the interface between lymphoma and normal tissue. The formation of immune synapses due to the derepression of the *IcosL* gene was also observed in the spleen of *miR-155*^{LSLrTA} mice, where a small, however increasing, percentage of B cells positive for IcosL was recorded, i.e., from 3.94% when *miR-155* was turned back OFF up to 13.94% 4 d later (*SI Appendix*, Fig. S6).

The Loss of *IcosL* Expression Is Also Associated with B Cell Malignant Transformation in Eμ-*miR-155* Mice. We next examined whether the targeting of IcosL by *miR-155* is part of a broader phenomenon. To this end, we examined the expression of IcosL in B cells from our Eμ-*miR-155* transgenic mice (4). Splenocytes from WT and Eμ-*miR-155* transgenic littermates were stained for CD19 and B220 B-cell surface markers and were then analyzed for IcosL expression using flow cytometry. Of note, CD19+ splenocytes from Eμ-*miR-155* transgenic express MHC-II based on flow cytometry analyses (*SI Appendix*, Fig. S7).

In addition, flow cytometry analysis of splenocytes from Eμ-*miR-155* transgenic mice showed the existence of both CD19+B220– and CD19+B220+ cell subpopulations. The expression of IcosL in CD19+B220+ B cells was slightly reduced in Eμ-*miR-155* mice. However, the expression of IcosL was completely lost in CD19+B220– cell subpopulation that was only found in Eμ-*miR-155* transgenic spleens (Fig. 3 *A* and *B*). Lymphomas from Eμ-*miR-155* mice were negative for both, B220 and IcosL expression based on IHC analyses (Fig. 3*C*). A highly malignant B220$^{low/-}$/CD19^{+} B cell immunophenotype was also reported by Yin et al. (30), when Bcor frameshift mutations were introduced in NP23 HSPCs. Interestingly, both, CD19+B220+ and CD19+B220– subpopulations in Eμ-*miR-155* transgenic mice, expressed elevated levels of PDL1, another immune checkpoint (31) (Fig. 3 *A* and *B*). Without excluding the possibility that PDL1 is also involved in immune escape, B cell malignancy in our mice, nevertheless, is likely to be due to the complete loss of IcosL in addition to the gain of PDL1 expression. Whether high levels of PDL1 are also involved in the loss of IcosL expression remains to be shown. Altogether, the data from flow cytometry and IHC showed that lymphoma cells in Eμ-*miR-155* transgenic mice do not express IcosL. In addition, the above data showed that while B220-positive and B220-negative

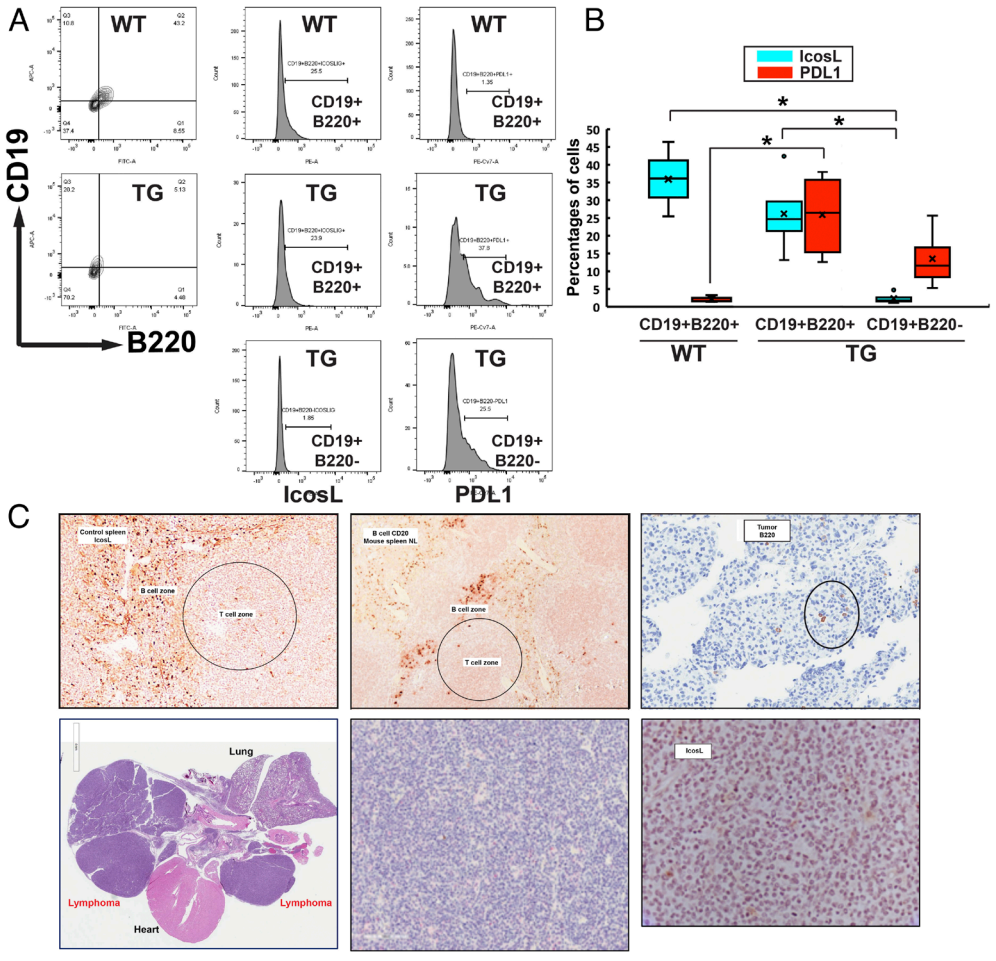

Fig. 3. Loss of *IcosL* expression as B cells progress toward malignancy in Eμ-*miR-155* mice. (*A*) Representative flow cytometry images of splenocytes from WT and Eμ-*miR-155* transgenic mice (TG) stained for CD19, B220, IcosL, and PDL1. Gated CD19+B220+ in WT and TG mice and CD19+B220- splenocytes in TG mice were analyzed for IcosL and PDL1 (two *Bottom* panels). *n* = 3/genotype. (*B*) Graphical presentation of the percentage of B cell subpopulations positive for IcosL or PDL1 analyzed in panel *A*. *n* = 3/group. **P* < 0.0285. (*C*) *Top* panels: *Left*, IcosL staining (brown) of a spleen section from a WT mouse. The circle indicates the T cell zone of the spleen; *Middle*, CD20 (brown) staining of a WT spleen; *Right*, lymphoma cells of Eμ-*miR-155* mice are B220 negative based on IHC. The circle indicates very few B220+ cells (brown) in this lymphoma. *Bottom* panels: *Left*, H&E staining of the chest organs of a terminally ill Eμ-*miR-155* mouse. *Middle*, the expression of IcosL (brown) is completely lost in lymphoma cells of TG Eμ-*miR-155* mouse; *Right*, Lymphoma cells from another terminally ill Eμ-*miR-155* mouse stained for IcosL (brown) were also negative for IcosL expression.

(lymphoma cells) in Eμ-*miR-155* mice express similar levels of PDL1, the two subpopulations could be distinguished by the loss of IcosL expression in malignant cells.

The Expression of *IcosL* in Malignant Cells Disrupts Tumor Development in Syngeneic C57BL6 Mice. The above data suggested that dysfunction of the ICOS–ICOSL immune checkpoint may play a critical role in B cell malignancies. To investigate this hypothesis, we devised a strategy aimed at assessing the ability of IcosL to induce tumor rejection when expressed in malignant B cells. Initially, we created a cell line from an Eμ-*miR-155* lymphoma, which as anticipated, did not express IcosL. Subsequently, these cells were transfected with either a construct containing an inducible tetracycline-responsive element upstream of a CMV-*IcosL* (Tet-on-CMV-*IcosL*), or a CMV-*IcosL* construct that constitutively expressed the mouse *IcosL* gene. The expression of *IcosL* by the Tet-on-CMV-*IcosL* or the CMV-*IcosL* constructs was tested by western blot analysis on lysates from transiently transfected HEK-293 cells, as indicated in *SI Appendix*, Fig. S8. It is important to note that the constructs used in this study only contained the coding region of the mouse *IcosL* gene, making the derived transcripts insensitive to *miR-155* activity. However, despite multiple attempts, we repeatedly observed that IcosL expression was progressively lost in lymphoma cells during their selection on G418-containing medium.

On the other hand, we have previously established that *miR-155* expression is significantly elevated in several solid tumors, including colon, breast, pancreatic, and lung cancer (10, 11). The C57BL6-derived MC38 colon cancer cell line (26) expressed extremely low levels of IcosL based on flow cytometry (Fig. 4*A*) and was therefore used in ensuing experiments. Ultimately, we utilized two transformants of the MC38 cell line that were transfected and selected on G418 to contain a CMV-*IcosL* vector. The A4 transformant served as a control, as it did not express IcosL, while the A5 transformant expressed high levels of IcosL based on flow cytometry analysis (Fig. 4*A*).

Subcutaneous injection of 1 million cells/per mouse, either MC38-A4 (control) or MC38-A5 (IcosL) was performed on the same day on six mice/experimental group (three males and three females). MC38-A4-derived tumors showed focal surface ulceration (arrowheads in Fig. 4*B*) indicative of rapid growth, a feature that was not found in mice injected with IcosL-expressing MC38-A5 cells. In addition, the tumors derived from MC38-A4 cells were significantly larger than tumors derived from MC38-A5 cells (Fig. 4*C*). Histopathological analysis using H&E staining showed extensive necrosis in control group, but much less in the IcosL-expressing tumors (Fig. 4*D* arrowheads in the *Top Left* panel). Additional images showing rapid overgrowth and necrosis in MC38-A4-derived tumors vs. a relative lack of necrosis in MC38-A5 tumors are shown in *SI Appendix*, Fig. S9. Unlike the tumors derived from MC38-A4 cells, MC38-A5-derived tumors that showed minimal necrosis, marked T cell infiltration, and presented with inflammatory infiltrates at the invading front of the tumor (Fig. 4*D* arrowhead in the *Bottom Left* panel). The flow cytometry analysis of tumors showed no difference in the percentage of CD4-positive cells in control and IcosL-expressing tumors, but there was a highly significant increase in the percentage of CD8-positive T cells in IcosL-expressing tumors (*SI Appendix*, Fig. S9). We therefore hypothesized that the inflammatory infiltrates in MC38-A5 cells-derived tumors were likely CD8-positive cytotoxic T cells. Therefore, we next analyzed the MC38-A4 and MC38-A5 tumors for both, IcosL and CD8 expression using IHC. As expected, many cells in MC38-A5 tumors stained positive for IcosL (Fig. 4 *D*, *Bottom Middle* panel; red signal). Importantly, the presence of IcosL-positive cells (red signal) in these tumors was paralleled by a concomitant heavy infiltration of cytotoxic CD8 T cells (Fig. 4 *D*, *Bottom Right* panel; brown signal). On the other hand, the CD8 infiltration was minimal in MC38-A4 control tumors, as was the expression of IcosL (Fig. 4 *D*, *Top Middle* and *Right* panels). Detailed coexpression analyses of CD8 and IcosL in the MC38-A5-derived tumors showed that in fact the CD8 T cells strongly concentrated in regions rich in IcosL-expressing cells (Fig. 4*E*), suggesting for a critical crosstalk taking place between the two cellular subsets. In addition, colocalization analyses showed that CD8-positive and IcosL-positive cells were indeed forming immunological synapses as evidenced by the yellow signals on the enlargements (E1 and E2) of the two red squares on the lower middle panel (Fig. 4*E*, third column). Interestingly, flow cytometry analysis for MC38-A5-tumors showed that a large part of injected cells had lost IcosL expression (*SI Appendix*, Fig. S10), indicating a selective pressure against the expression of the *IcosL* gene, that enabled these cells to escape the immune surveillance. This argument is further supported by the fact that although a rare event, we did find areas with few CD8-positive and IcosL-positive cells in MC38-A5-derived tumors (*SI Appendix*, Fig. S11). Of note, IHC staining, and analyses were done blinded of the tumor origin and performed by investigators different from those that performed the flow cytometry analysis. Overall, the reduced size of the tumors, the enhanced presence of CD8-positive T cells in the vicinity of IcosL-expressing cells, and the formation of synapse between these two cell types in MC38-A5-derived tumors suggested a genuine immune response toward MC38 IcosL-expressing cells in C57BL6 mice, in contrast to MC38 cells that did not express IcosL.

Discussion

We have previously shown that overexpressing *miR-155* in B cells under the *E*μ-enhancer results in the development of aggressive B cell malignancies (4). Similarly, inducing *miR-155* expression in lymphoid tissue using a tetracycline-inducible system led to the formation of aggressive B cell lymphomas [(5), and this manuscript]. However, lymphoma infiltrates rapidly disappeared when *miR-155* expression was turned back OFF in 155^{LSLrTA} mice (this manuscript). The disappearance of malignant infiltrates coincided with an increased infiltration of T cells, leading us to consider the possibility that high levels of *miR-155* in B cells may impair T cell recruitment to the tumor site as well as B-T cell interactions. This prompted us to search for surface antigens that are both expressed by B cells and predicted targets of *miR-155*. We focused on the ICOSL checkpoint and found that in two mouse models of *miR-155*-induced lymphomas, the malignant cells were negative for IcosL. In addition, turning *miR-155* back OFF in $miR\text{-}155^{LSLrTA}$ mice led to reappearance of benign B cells re-expressing IcosL and forming immunological synapses with T cells through IcosL–Icos interactions. It is also worth emphasizing that as B cells from Eμ-*miR-155* mice progressed toward a more aggressive phenotype, both the premalignant and malignant B cells kept expressing PDL1 at similar levels and thus could not be differentiated based on PDL1 expression alone. However, these two kinds of cells could be discriminated by the level of IcosL expression, with the malignant B cells showing complete loss of IcosL. Finally, we provide strong evidence that IcosL is a genuine target of *miR-155* based on Luciferase assays, *miR-155* overexpression, inhibition of IcosL expression, and by assessing both, IcosL and *miR-155* expression in two different types of B cell malignancies, CLLs and BLs.

CLLs originate from mature naïve B cells that have not yet encountered antigens (32), while BL cells arise from GC B cells that have already encountered T cell-dependent antigens (33). Activated

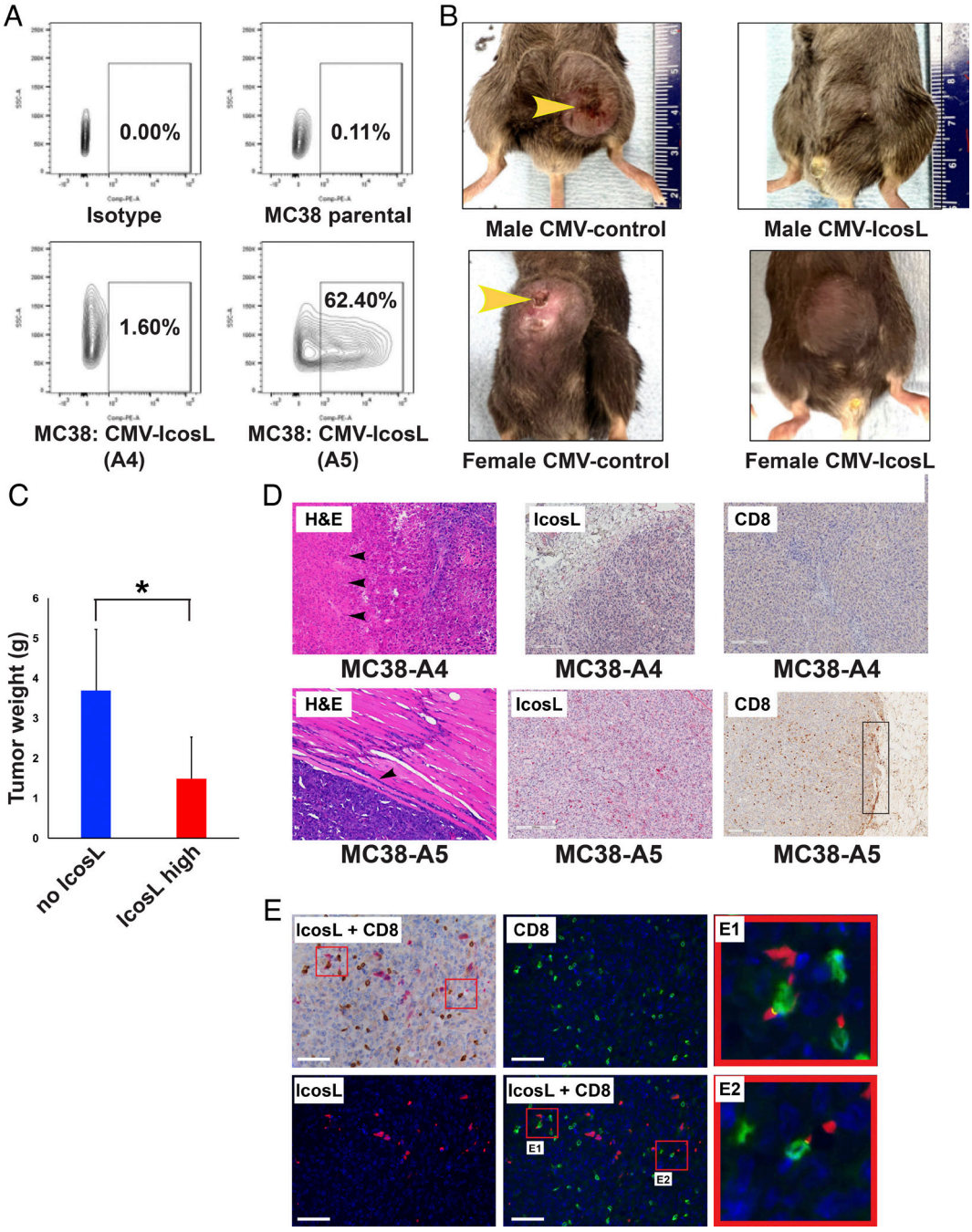

Fig. 4. Expression of *IcosL* in MC38 colon tumor cells injected subcutaneously causes tumor regression. (*A*) Flow cytometry analysis of IcosL expression in parental MC38 cells, and MC38 cells transfected with the CMV-IcosL vector and selected on G418-containing medium for the expression of the neomycin gene present in the CMV-IcosL vector. MC38-A4 cells do not express IcosL and were further used as control, while MC38-A5 express high levels of IcosL. (*B*) Tumors originating from mice injected with MC38-A4 cells are larger than those injected with MC38-A5 cells and show skin ulceration indicated by arrowheads. (*C*) The size in grams of tumors originating from MC38-A4 and MC38-A5 transformants was significantly different. $P = 0.0286$. $n = 5$ for MC38-A4 tumors, as one female was found dead and was not included in the experiment; $n = 6$ for MC38-A5 tumors. (*D*) Histopathological and cellular characterization of tumors derived from MC38-A4 and MC38-A5 cells. Extensive necrosis indicative of rapid growth in tumors derived from MC38-A4 cells (arrowheads in the *Top Left* panel). Less necrosis and presence of inflammatory infiltrates at the invading front of the tumor in tumors derived from MC38-A5 cells (arrowhead in the *Lower Left* panel). The two middle panels in each row show staining for IcosL, with minimal expression found in MC38-A4 tumors and many IcosL positive (red) present in MC38-A5 tumors ($P = 0.0001$). The two *Right* panels in each row show staining for CD8 with significantly higher infiltration of CD8-positive cells (brown) in MC38-A5 and minimal CD8-positive cell infiltration in control MC38-A4 tumors ($P = 0.0015$). The *Right Bottom* panel also shows massive CD8-positive T cell infiltration at the border of tumor growth (rectangle). (*E*) Coexpression analysis based on the immunofluorescence signals of IcosL and CD8 in the heavy CD8-infiltrated areas of MC38-A5 tumors. *Top Left* panel: The expression of IcosL (red) and CD8 (brown) under visible light; *Top Middle* panel: CD8-positive cells (green); *Bottom Left* panel: IcosL expression (red); *Middle Bottom* panel: Coexpression of CD8 and IcosL. (Scale bars, 100 μm.) E1 and E2 are enlargements of the red squares in the bottom middle panel where due to the close vicinity of IcosL-positive and CD8 cells the overlay of the two signals becomes yellow.

B cells in GC express high levels of IcosL that facilitates their interactions with T follicular helper cells through Icos (34). Such B-T cell interactions are vital for the development of high affinity antibody responses, class switching, and the generation of long-lived plasma cells and memory B cells (35). *MiR-155* also is a critical player in immune responses within GC B cells. Namely, in addition to promoting B cell survival and proliferation, *miR-155* controls somatic hypermutation and class switch recombination in GC B cells by targeting AICD (Activation-Induced Cytidine Deaminase) (36). Dynamic changes in *miR-155* expression are thus expected to occur

during B cell maturation, in particular, the transient decrease of *miR-155* levels needed to allow the expression of AICD and ICOSL upon B cell activation. Thus, single-cell sequencing of B cells from the GCs showed that *miR-155HG* (the host gene from which *miR-155* primary transcript is produced) is expressed at different levels in the different B cell clusters identified by Holmes et al. (37). Therefore, genomic alterations or other molecular malfunctions that disrupt the tight control of the expression of *miR-155*, IcosL, or other critical factors controlling B cell maturation may potentially contribute to the development of distinct tumors, such as CLL and BL.

Our findings indicate not only that IcosL acts as a costimulatory factor for T cells during the late stages of the immune response after T cells have reached the inflamed tissues, as previously reported (38), but that IcosL also plays a crucial role in promoting T cell recruitment at the tumor site. Thus, in two different cancer models, we found that the re-expression of IcosL by B cells or the overexpression of IcosL in MC38 tumor cells significantly increased both, T cell infiltration, the formation of immunological synapses between T cells and cancer cells, and the elimination of malignant cells. Injecting mice with MC38 cells that expressed IcosL led to substantial infiltration of tumors by CD8-positive cells and delayed the onset of terminal illness. These results indicate that IcosL activity in tumor cells can make them more responsive to anticancer immunity, pointing to a critical role of IcosL in the effectiveness of antitumor immune responses. This is in accordance with previous studies showing that: 1) Patients with higher levels of *IcosL* transcripts have a better prognosis for nasopharyngeal carcinomas (39); 2) The activation of the Icos–IcosL signaling pathway in colon cancer is associated with improved survival (40); and 3) Chemotherapies enhance IcosL expression in the B cells of breast cancer patients, thereby improving survival outcomes (41). This better outcome was attributed to the greater recruitment of cytotoxic T cells by IcosL-expressing B cells (42).

T cell responses elicited by the Icos–IcosL costimulatory pathway have been shown to be critical for both, CD4+ T cell regulatory activities, and CD8+ cytotoxic T cell responses (43). Our results critically establish that the effects of ICOSL on T cells vary depending on the type of malignant cells being recognized and eliminated. Namely, in B cell malignancies, IcosL effects primarily increased the capability of CD4+ T cells to form immune synapses with B cells through Icos–IcosL interactions. Furthermore, flow cytometry analysis of B cells from Eμ-*miR-155* mice showed that CD19+ cells actually express MHC-II, which can explain a CD4-T cell-based response. In contrast, the immune response to MC38 solid tumor cells that were expressing IcosL was mostly mounted by CD8+ T cells, with no detectable effects on the size of CD4+ T cell population within the tumor. Different groups have shown that MC38 cells express H-2K^b class I MHC (44) as well as MHC-I-restricted antigens (45). In addition, similar to our work, a CD8-response toward MC38 cells has been reported (44). On the other hand, research on possible effects of ICOSL or *miR-155* on the expression of MHC-I and MHC-II genes should be the subject of interesting studies in the future. Nevertheless, in two different mouse models, solid tumor, and B-cell lymphoma, we observed an enhanced T cell infiltration in response to IcosL expression by malignant cells followed by synapse formation between T (Icos)-cancer (IcosL) cells and the elimination of these malignant cells.

Overall, in our study, the manipulation of *miR-155* expression levels was essential to understanding the deleterious consequences of the targeting of *IcosL* transcripts by *miR-155*. Our findings thus establish IcosL as a critical factor in immune rejection of tumors by boosting host antitumor immunity and show that the targeting of *IcosL* transcripts by *miR-155* is instrumental in tumor development. Our finding has important implications not only for T-cell-based immune therapies of B-cell malignancies but also of common solid tumors that exhibit high levels of *miR-155*, such as lung, breast, pancreatic, and colon cancer. By harnessing the potential of Icos–IcosL immune checkpoint to enhance the body's immune response, either by blocking *miR-155* activity or by re-expressing *IcosL* gene, we will have the opportunity to markedly enhance the efficacy of cancer treatments. Our findings suggest that ICOS–ICOSL checkpoint could be a critical target for future immune therapies.

Materials and Methods

Mice. Eμ-*miR-155* mice have been previously described (4). *miR-155* Cre-loxP tetracycline-controlled knock-in mouse model, *miR-155*^{LSLtTA}, in which *miR-155* is targeted to the *ROSA26* locus, were donated by Dr. Slack and are described in the publication by Babar et al. (5). They were mated to *Nestin*-Cre mice (Jax. Org; Catalog number 003771). Doxycycline withdrawal was done at day P1. Littermates from parallel mating fed with Doxycycline were used as control. Doxycycline Grain-Based Rodent Diet, Sterile, was purchased from Bio-Serv (Catalog No. S3888).

DNA Constructs. Preparation of ICOSL-luciferase reporter clones. A 492 bp-long fragment of human *ICOSL* 3′-UTR (corresponding to nucleotides 2,321 to 2,812 of NCBI Reference Sequence: NM_015259.6) that contains the putative target site for *miR-155-5p* was cloned downstream of the *Renilla* luciferase gene in the psiCHECK2 vector (Promega). The construct containing the mutated/deleted *miR-155* target site (AGCATTA) (psiCHECK2-*ICOSL*_Mut) was built based on this construct. Specifically, the putative *miR-155-5p* site was replaced by six nucleotides that constitute the EcoR1 restriction site (GAATTC). The sequences of the DNA oligonucleotides used to create these two constructs are

ICOSLG_Dir 5′-GGCTCGCTCGAGCCCTCCTTCTTACTTCCCAG-3′
ICOSLG_Rev 5′-AGAGTCGCGGCCGCCCCAGGGCACCTCCCGGGAC-3′
ICOSLG_MUT_DIR 5′-GAAGAATTCGAAGATGTGTGGTGTTTATAAAAG-3′
ICOSLG_MUT_REV 5′-TTCGAATTCTTCATGTTAAAAGCGGGAGTG-3′

For preparing the psiCHECK2-*ICOSL*_Mut/deletion, we first PCR amplified two fragments of the WT 3′-UTR of *ICOSL* that correspond to the upstream and downstream regions of the *miR-155* binding site and introduced an *Eco*RI restriction enzyme cutting site (GAATTC). Specifically, the ICOSLG_Dir and ICOSLG_MUT_REV oligonucleotides were used to obtain the 5′-part of ICOSLG sequence and ICOSLG_MUT_DIR and ICOSLG_Rev oligonucleotides were used to obtain the 3′-part of ICOSLG sequence. The two fragments were then digested with the *Eco*RI enzyme and ligated, replacing the *miR-155* binding site with the GAATTC sequence. This strategy was designed due to the difficulty of directly mutating the *miR-155* binding-site in *ICOSL* 3′-UTR due to the great richness in adenine and thymine of sequences surrounding the site. The deletion of the *miR-155* binding site or the introduction of the SNP was confirmed by sequencing.

Flow Cytometry. Flow cytometry analyses were done on single-cell suspension of either spleen, lymph nodes, peritoneal lymphomas, MC38 cell grown in culture, and MC38-A4- or MC38-A5-derived tumors. Splenocytes were treated with red blood cell lysis buffer (Sigma) for 5 min on ice prior to staining. After tissues were smashed using the plungers of a 1 mL syringes, they were passed through cell strainers, to prepare single-cell suspensions. Staining was always done in parallel for transgenic and WT littermate mice, or for MC38-A4, MC38-A5 tumors. Antibodies were as follow: anti-CD3-APC: 17-0031-81, eBioscience; anti-CD3-PeCy7: 25-0031-81, eBioscience; anti-CD4-APC: 561091, BD-Bioscience; anti-CD4-PE: 12-0041-82, eBioscience; anti-CD4-PeCy7: 563933, BD-Bioscience; anti-CD8-PeCy7: 25-0081-81, eBioscience; anti-CD8-FITC: 11-0081-82, eBioscience; anti-CD19: 17-0193-82, eBioscience; anti-B220-APC: 17-0452-81, eBioscience; anti-B220-PeCy7: 552772, BD-Bioscience, anti-B220-FITC: 11-0452-82, eBioscience; anti-IcosL-PE: 12-5985-82, eBioscience; anti-Icos-APC: 17-9949-82, eBioscience; anti-Icos-FITC: 11-9942-82, eBioscience; anti-PD1-FITC: 11-9985-81, eBioscience; anti-PDL1-PeCy7: 25-5982-80, eBioscience. Samples were analyzed on a Calibur (BD-Biosciences) machine. Data were analyzed using FloJow software (Ashland, OR).

Immunohistochemistry (IHC) and ISH. Tissues were fixed in 4% formalin for at least 48 h before further processing. Fixed tissues were embedded into paraffin blocks, sectioned, and placed into microscopic slides at the Comparative Pathology and Digital Imaging Shared Resource, Department of Veterinary Biosciences, College of Veterinary Medicine, The Ohio State University, as pay per service. Staining for CD4, CD8, B220, and H&E were done in this facility.

Reagent used were Primary antibodies: CD4 (Abcam; ab183685; 0.25 μg/mL); CD8 (Cell Signaling; CST98941; 2 μg/mL); CD45R (BD Biosciences; 550286; 0.125 μg/mL). Secondary antibody: Horse Anti-Rabbit (Vector Laboratories; MP-7401; ready to use); Goat Anti-Rat (Vector Laboratories; MP-5444; ready to use); Substrate DAB Dako (K3468, as per manufacturer recommendation); ImmPACT (Vector Red Vector Laboratories; SK-5105; as per manufacturer recommendation); endogenous enzyme block BLOXALL (Vector Laboratories; SP-6000; ready to use); Protein block: Normal Horse Serum (Vector Laboratories; MP-7401; ready to use); Normal Goat Serum (Vector Laboratories; MP-5444, ready to use); Antigen retrieval buffer: Target Retrieval Solution Dako; S2367; 1X.

IHC for specific antibodies such as ICOS, ICOSL, CD163, CD3, and CD20, and the ISH for *miR-155* were done by Dr. Nuovo, as previously reported (46–48). The specific antibodies used (source and catalog numbers) were as follows: ICOS (ProSci; 8685), ICOSL (ProSci; 8687), T cell (CD3) (Abcam; ab16669), CD163 (Abcam; ab182422), CD31 (Abcam; ab28364); and CD20 B cells (Biogenex; AM537GP). All required pretreatments (antigen retrieval) were done for 30 min at 95 °C using an EDTA solution. The IHC protocol used the Leica Bond Max (Buffalo Grove, IL) automated platform; the Fast Red (DS 9820) and the DAB (DS 9800) detection kits gave equivalent results. The protocol for ISH for microRNAs has also been previously reported in detail (49). All sections were dealt with blindly using an automated Leica Bond Max platform. Coexpression analyses were done using the Nuance system (CRI) as previously published (48). Tissues/slides were first stained for two different targets of interest using Fast Red, NBT/BCIP or DAB as the chromogens. Coexpression experiments were performed by analyzing a given tissue section for one protein using the DAB (brown) chromogen and analyzing the other protein with Fast Red chromogen. Colocalization of the signals was then analyzed by the Nuance and InForm advanced image analyses software systems (PerkinElmer) with the Zeiss Axioskop microscope (48). Quantification for the signal with either single IHC or multilabeled IHC was done using either InForm software or manual counting which yielded equivalent results. IHC scoring for Fig. 4 was done blinded to the treatment regimens. The optimal conditions for ICOSLG (ProSci, #8687) and CD8 (ABCAM, #ab316778) were each pretreatment for 30 min with an EDTA antigen retrieval solution (pH 9.0). Three 200X fields were analyzed for a given tumor with each field scored for the number of cells with the target of interest. This allowed the analysis of over 75% of each tumor.

qRT-PCR. RNAs were extracted either with TRIzol (Life Technologies) or the RNA purification kit from Norgen (Thorold, ON, Canada). MicroRNA and gene qRT-PCRs were respectively performed using the corresponding Assays from Life Technologies as follows: Actin-β (mouse) Taqman gene expression assay (Mm00607939_s1); Actin-β Taqman (human) gene expression assay (HS03023943_g1); Hsa-*miR-155* Taqman miRNA assay (002623); Mmu-*miR-155* Taqman miRNA assay (002571); Control miRNA Assay U6 snRNA (001973); ICOSL: HS01055793_m1; IcosL: Mm00497237_m1; Icos: Mm00497600_m1; Values were normalized using *U6* for microRNAs assays, and β-Actin or GAPDH for gene expression assays. The cDNA synthesis for gene expression assays was set up on 1 μg RNA. Ten nanogram RNAs were used as starting material for microRNA qRT-PCR assays. The high-capacity cDNA reverse transcriptase kit with RNA inhibitor was used to prepare the cDNAs, Catalog No.: 4368814. Taqman Fast Universal PCR Master Mix Catalog No. 4367846.

Western Blot. Protein lysates were run on ready-to-use 4 to 20% gradient agarose gels from Biorad. Antibodies were as follow: IcosL: Abcam (ab209262, 1:500 dilution); Icos: Abcam (ab224644, 1:500 dilution); α-Tubulin: Cell Signaling Technologies (CST9099, 1:1,000 dilution); β-actin: Cell Signaling Technologies (CST3700, 1:1,000 dilution); GAPDH: GeneTex, (Gtx627408, 1:1,000 dilution); SOCS1: Abclonal (A7754, 1:500 dilution).

Luciferase Assays. Cells were plated a night before transfection in 24-well plates. Transfection was done using Lipofectamine following standard protocols as suggested by the manufacturer. Whenever needed, cells were treated 24 h posttransfection. Luciferase assays were run 48 h after transfection as previously described (49). The luciferase activity was read on a Luminometer (Promega), using The Dual-Luciferase® Reporter (DLR™) Assay System.

Cell Lines and DNA/microRNA Transfection. THP-1 and Raw264.7 cells were purchased from ATCC. Cells were grown following standard procedures in RPMI1640 medium supplemented with heat-inactivated bovine fetal serum at concentration 10% and penicillin/streptomycin. The MC38 cell line was established in the laboratory of Dr. Jeffrey Schlom at NCI (26). This cell line has a high mutation burden. All reagents for tissue culture were purchased from Sigma. LPS and phorbol 12-myristate 13-acetate (PMA) were purchased from Sigma, diluted in PBS as stock, and used as previously reported (27). Raw264.7 and HEK-293 cells were transfected using Lipofectamine 2000 (Invitrogen). MC38 cells were transfected with JetPei Polyplus using the manufacturer's instructions with some modifications. One million cells were seeded in a 10 cm dish and the next day transfected with two micrograms of CMV-mouse IcosL plasmid and 6 μL of JetPei transfection reagent. Two days later the cells were seeded in a 15 cm dish with medium containing 800 μg/mL of G418. Single colonies were isolated and expanded with continued selection (final concentration of G418 400 μg/mL) and tested for IcosL expression by flow cytometry. Clone A4 (nonexpressing) and clone A5 were used for mouse tumor studies. THP-1, BL, and CLL cell lines were electroporated using Amaxa® Cell Line Nucleofector® Kit V from Lonza. Mouse *miR-155* RNA was used to transfect Raw264.7, while the rest of the cells (BLs, CLLs, THP-1, and HEK-293 were transfected with human *miR-155*-RNA. MicroRNAs were transfected at 100 nM final concentration. MicroRNAs, purchased from Ambion/Life technologies, are as follows: PM13058 Pre-miR miRNA Precursors mmu-miR-155; AM13058 Anti-miR miRNA Inhibitors mmu-*miR-155-5p*; AM17110 Pre-miR™ miRNA Precursor Negative Control #1; AM17010 Anti-miR™ miRNA Inhibitor Negative Control #1; AM12601 Pre-miR miRNA Precursors Hsa-miR-155; PM12601 Anti-miR miRNA Inhibitors Hsa-*miR-155-5p*. HEK-293 cells were plated on 6-well plates and transfected with either CMV-*mIcosL* or pENTRY-rtTA-*mIcosL* clone using Lipofectamine 2000 (Invitrogen). The expression of *mIcosL* in cells transfected with the pENTRY-rtTA-*mIcosL* clone was induced 48 h later using doxycycline 1 μg/mL. The expression of mIcosL was checked 48 h postdoxycycline treatment using western blot.

Statistical analyses. They were done using the Student *t* test, and *P* values are provided in the figure legends. The multispectral and coexpression statistical analyses were done using InStat Statistical Analysis Software (version 3.36) and a paired *t* test (also referred to as a "repeated measure *t* test"). The null hypothesis was rejected if the significance level was below 5%.

MicroRNA Predicted Site Analyses. In silico analysis to identify the microRNAs that can potentially target *ICOSL* transcripts was done using Targetscan.org software (50).

Data, Materials, and Software Availability. All study data are included in the article and/or *SI Appendix*.

ACKNOWLEDGMENTS. This work was supported by CLL Global Research Foundation Awards AWD-115284 and AWD-116510 to C.M.C. Genomics Shared Resource and Flow Cytometry facility, part of Comprehensive Cancer Center is an NCI subsidized Shared Resource and is supported by CCSG: P30CA016058 Grant. We want to thank Dr. J. Schlom (NCI) for generously providing us with the MC38 cell line; and Dr. T. Nakamura for cloning the mouse *IcosL*-cDNA into the pEntry-Tet-on-CMV vector.

Author affiliations: [a]Department of Anesthesiology, Wexner Medical Center, College of Medicine, The Ohio State University, Columbus, OH 43210; [b]The Ohio State University, Comprehensive Cancer Center, Department of Cancer Biology and Genetics, Wexner Medical Center, Columbus, OH 43210; and [c]GNOME, Inc., Powell, OH 43065

1. G. A. Calin *et al.*, A MicroRNA signature associated with prognosis and progression in chronic lymphocytic leukemia. *N. Engl. J. Med.* **353**, 1793–1801 (2005).
2. B. Cui *et al.*, MicroRNA-155 influences B-cell receptor signaling and associates with aggressive disease in chronic lymphocytic leukemia. *Blood* **124**, 546–554 (2014).
3. S. G. Papageorgiou *et al.*, MicroRNA-155-5p overexpression in peripheral blood mononuclear cells of chronic lymphocytic leukemia patients is a novel, independent molecular biomarker of poor prognosis. *Dis. Markers* **2017**, 2046545 (2017).
4. S. Costinean *et al.*, Pre-B cell proliferation and lymphoblastic leukemia/high-grade lymphoma in E(mu)-miR155 transgenic mice. *Proc. Natl. Acad. Sci. U.S.A.* **103**, 7024–7029 (2006).
5. I. A. Babar *et al.*, Nanoparticle-based therapy in an in vivo microRNA-155 (miR-155)-dependent mouse model of lymphoma. *Proc. Natl. Acad. Sci. U.S.A.* **109**, E1695–E1704 (2012).
6. S. Costinean *et al.*, Src homology 2 domain-containing inositol-5-phosphatase and CCAAT enhancer-binding protein beta are targeted by miR-155 in B cells of Emicro-MiR-155 transgenic mice. *Blood* **114**, 1374–1382 (2009).

7. R. M. O'Connell, A. A. Chaudhuri, D. S. Rao, D. Baltimore, Inositol phosphatase SHIP1 is a primary target of miR-155. *Proc. Natl. Acad. Sci. U.S.A.* **106**, 7113–7118 (2009).
8. I. M. Pedersen *et al.*, Onco-miR-155 targets SHIP1 to promote TNFalpha-dependent growth of B cell lymphomas. *EMBO Mol. Med.* **1**, 288–295 (2009).
9. A. Androulidaki *et al.*, The kinase Akt1 controls macrophage response to lipopolysaccharide by regulating microRNAs. *Immunity* **31**, 220–231 (2009).
10. S. Volinia *et al.*, A microRNA expression signature of human solid tumors defines cancer gene targets. *Proc. Natl. Acad. Sci. U.S.A.* **103**, 2257–2261 (2006).
11. M. Bloomston *et al.*, MicroRNA expression patterns to differentiate pancreatic adenocarcinoma from normal pancreas and chronic pancreatitis. *JAMA* **297**, 1901–1908 (2007).
12. Y. Wu *et al.*, The diagnostic and prognostic value of miR-155 in cancers: An updated meta-analysis. *Mol. Diagn. Therapy* **27**, 283–301 (2023).
13. W. Kong *et al.*, Upregulation of miRNA-155 promotes tumour angiogenesis by targeting VHL and is associated with poor prognosis and triple-negative breast cancer. *Oncogene* **33**, 679–689 (2014).
14. K. Van Roosbroeck *et al.*, Combining anti-Mir-155 with chemotherapy for the treatment of lung cancers. *Clin. Cancer Res.* **23**, 2891–2904 (2017).
15. H. Shibuya *et al.*, Clinicopathological and prognostic value of microRNA-21 and microRNA-155 in colorectal cancer. *Oncology* **79**, 313–320 (2010).
16. M. Mikamori *et al.*, MicroRNA-155 controls exosome synthesis and promotes gemcitabine resistance in pancreatic ductal adenocarcinoma. *Sci. Rep.* **7**, 42339 (2017).
17. A. Hutloff *et al.*, ICOS is an inducible T-cell co-stimulator structurally and functionally related to CD28. *Nature* **397**, 263–266 (1999).
18. G. J. Freeman *et al.*, Cloning of B7–2: A CTLA-4 counter-receptor that costimulates human T cell proliferation. *Science* **262**, 909–911 (1993).
19. S. K. Yoshinaga *et al.*, T-cell co-stimulation through B7RP-1 and ICOS. *Nature* **402**, 827–832 (1999).
20. A. J. Coyle *et al.*, The CD28-related molecule ICOS is required for effective T cell-dependent immune responses. *Immunity* **13**, 95–105 (2000).
21. A. Tafuri *et al.*, ICOS is essential for effective T-helper-cell responses. *Nature* **409**, 105–109 (2001).
22. T. W. Mak *et al.*, Costimulation through the inducible costimulator ligand is essential for both T helper and B cell functions in T cell-dependent B cell responses. *Nat. Immunol.* **4**, 765–772 (2003).
23. C. Dong *et al.*, ICOS co-stimulatory receptor is essential for T-cell activation and function. *Nature* **409**, 97–101 (2001).
24. L. Liang, E. M. Porter, W. C. Sha, Constitutive expression of the B7h ligand for inducible costimulator on naive B cells is extinguished after activation by distinct B cell receptor and interleukin 4 receptor-mediated pathways and can be rescued by CD40 signaling. *J. Exp. Med.* **196**, 97–108 (2002).
25. R. I. Nurieva *et al.*, B7h is required for T cell activation, differentiation, and effector function. *Proc. Natl. Acad. Sci. U.S.A.* **100**, 14163–14168 (2003).
26. T. H. Corbett *et al.*, Tumor induction relationships in development of transplantable cancers of the colon in mice for chemotherapy assays, with a note on carcinogen structure. *Cancer Res.* **35**, 2434–2439 (1975).
27. E. Tili *et al.*, Modulation of miR-155 and miR-125b levels following lipopolysaccharide/TNF-alpha stimulation and their possible roles in regulating the response to endotoxin shock. *J. Immunol.* **179**, 5082–5089 (2007).
28. J. Kluiver *et al.*, Lack of BIC and microRNA miR-155 expression in primary cases of Burkitt lymphoma. *Genes, Chromosomes Cancer* **45**, 147–153 (2006).
29. E. Tili *et al.*, Quaking and miR-155 interactions in inflammation and leukemogenesis. *Oncotarget* **6**, 24599–24610 (2015).
30. M. Yin *et al.*, Engineered Bcor mutations lead to acute leukemia of progenitor B-1 lymphocyte origin in a sensitized background. *Blood* **133**, 2610–2614 (2019).
31. P. Sharma *et al.*, Immune checkpoint therapy–Current perspectives and future directions. *Cell* **186**, 1652–1669 (2023).
32. T. J. Kipps *et al.*, Chronic lymphocytic leukaemia. *Nat. Rev. Dis. Primers* **3**, 16096 (2017).
33. K. Basso, R. Dalla-Favera, Germinal centres and B cell lymphomagenesis. *Nat. Rev. Immunol.* **15**, 172–184 (2015).
34. D. Liu *et al.*, T-B-cell entanglement and ICOSL-driven feed-forward regulation of germinal centre reaction. *Nature* **517**, 214–218 (2015).
35. C. D. Allen, T. Okada, J. G. Cyster, Germinal-center organization and cellular dynamics. *Immunity* **27**, 190–202 (2007).
36. Y. Dorsett *et al.*, MicroRNA-155 suppresses activation-induced cytidine deaminase-mediated Myc-Igh translocation. *Immunity* **28**, 630–638 (2008).
37. A. B. Holmes *et al.*, Single-cell analysis of germinal-center B cells informs on lymphoma cell of origin and outcome. *J. Exp. Med.* **217**, e20200483 (2020).
38. X. Liu *et al.*, B7H costimulates clonal expansion of, and cognate destruction of tumor cells by, CD8(+) T lymphocytes in vivo. *J. Exp. Med.* **194**, 1339–1348 (2001).
39. G. Zhang, Y. Xu, S. Zhang, H. Zhou, The ICOSL expression predicts better prognosis for nasopharyngeal carcinoma via enhancing oncoimmunity. *BioMed. Res. Int.* **2020**, 9756732 (2020).
40. O. Marinelli *et al.*, ICOS-L as a potential therapeutic target for cancer immunotherapy. *Curr. Protein Pept. Sci.* **19**, 1107–1113 (2018).
41. Y. Lu *et al.*, Complement signals determine opposite effects of B cells in chemotherapy-induced immunity. *Cell* **180**, 1081–1097.e24 (2020).
42. J. J. Wallin, L. Liang, A. Bakardjiev, W. C. Sha, Enhancement of CD8+ T cell responses by ICOS/B7h costimulation *J. Immunol.* **167**, 132–139 (2001).
43. L. Roussel *et al.*, Loss of human ICOSL results in combined immunodeficiency. *J. Exp. Med.* **215**, 3151–3164 (2018).
44. K. A. Paramitasari, I. Yasumasa, Sensitization with an allogeneic MHC class I molecule induces anti-tumor immunity in the absence of PD-1 in mice. bioRxiv [Preprint] (2023). https://doi.org/10.1101/2023.08.26.554968 Accessed 30 May 2024.
45. M. Yadav *et al.*, Predicting immunogenic tumour mutations by combining mass spectrometry and exome sequencing. *Nature* **515**, 572–576 (2014).
46. G. J. Nuovo *et al.*, A standardization protocol for the in situ detection of SARS-CoV2 RNA and proteins. *Appl. Immunohistochem. Mol. Morphol.* **30**, 83–90 (2022).
47. G. J. Nuovo, "Introduction" in *In Situ Molecular Pathology and Co-Expression Analyses*, G. J. Nuovo, Ed. (Academic Press ScienceDirect, Elsevier Inc., 2021), pp. 1–6.
48. G. J. Nuovo *et al.*, A methodology for the combined in situ analyses of the precursor and mature forms of microRNAs and correlation with their putative targets. *Nat. Protoc.* **4**, 107–115 (2009).
49. E. Tili *et al.*, GAM/ZFp/ZNF512B is central to a gene sensor circuitry involving cell-cycle regulators, TGF{beta} effectors, Drosha and microRNAs with opposite oncogenic potentials. *Nucleic Acids Res.* **38**, 7673–7688 (2010).
50. S. E. McGeary *et al.*, The biochemical basis of microRNA targeting efficacy. *Science* **366**, eaav1741 (2019).